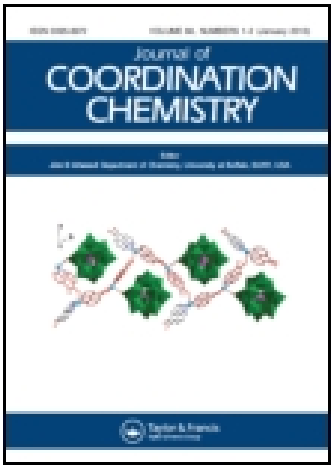

Journal of Coordination Chemistry
Publication details, including instructions for authors and subscription information:
http://www.tandfonline.com/loi/gcoo20

Copper(II), nickel(II), and ruthenium(III) complexes of an oxopyrrolidine-based heterocyclic ligand as anticancer agents

Waseem A. Wani[a], Zeid Al-Othman[b], Imran Ali[a], Kishwar Saleem[a] & Ming-Fa Hsieh[c]

[a] Department of Chemistry, Jamia Millia Islamia (Central University), New Delhi, India

[b] Department of Chemistry, College of Science, King Saud University, Riyadh 11451, Kingdom of Saudi Arabia

[c] Department of Biomedical Engineering, Chung Yuan Christian University, Chung Li, Taiwan

Accepted author version posted online: 16 Jun 2014.Published online: 31 Jul 2014.

To cite this article: Waseem A. Wani, Zeid Al-Othman, Imran Ali, Kishwar Saleem & Ming-Fa Hsieh (2014) Copper(II), nickel(II), and ruthenium(III) complexes of an oxopyrrolidine-based heterocyclic ligand as anticancer agents, Journal of Coordination Chemistry, 67:12, 2110-2130, DOI: 10.1080/00958972.2014.931947

To link to this article: http://dx.doi.org/10.1080/00958972.2014.931947

Journal of Coordination Chemistry, 2014
Vol. 67, No. 12, 2110–2130, http://dx.doi.org/10.1080/00958972.2014.931947

Copper(II), nickel(II), and ruthenium(III) complexes of an oxopyrrolidine-based heterocyclic ligand as anticancer agents

WASEEM A. WANI†, ZEID AL-OTHMAN‡, IMRAN ALI*†, KISHWAR SALEEM† and MING-FA HSIEH§

†Department of Chemistry, Jamia Millia Islamia (Central University), New Delhi, India
‡Department of Chemistry, College of Science, King Saud University, Riyadh 11451, Kingdom of Saudi Arabia
§Department of Biomedical Engineering, Chung Yuan Christian University, Chung Li, Taiwan

(*Received 20 December 2013; accepted 1 May 2014*)

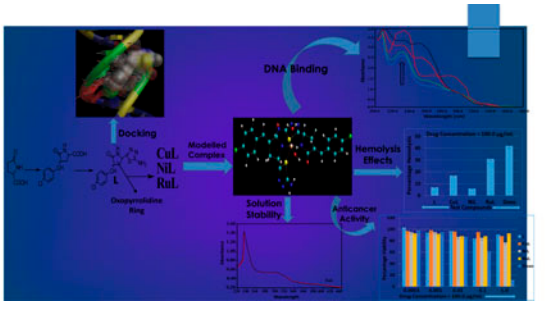

An oxopyrrolidine-based ligand [3-(4-chlorobenzylidine)-5-(5-amino-1,3,4-thiadiazol-2-yl)pyrrolidin-2-one] was synthesized by coupling pyroglutamic acid with *p*-chlorobenzaldehyde followed by cyclization with thiosemicarbazide in presence of oxyphosphoryl chloride. Copper, nickel, and ruthenium complexes of the ligand were also synthesized. The electrolytic nature, with octahedral geometries for nickel and ruthenium complexes, was observed, while tetragonally distorted octahedral geometry for copper complex was proposed. The complexes were resistant to dissociation and degradation in 5% DMSO solutions of PBS (pH 7.4). DNA binding constants (K_b) for ligand, copper, nickel, and ruthenium complexes were 1.15×10^5, 1.67×10^5, 1.87×10^5, and $1.007 \times 10^6\ M^{-1}$, respectively, indicating quite strong binding with DNA. *In silico* studies also showed that the ligand interacted with DNA mainly through van der Waal's forces. The docking energy of ligand−DNA adduct was –30.45 kJ M^{-1}, suggesting a good affinity of the reported ligand with DNA. Both the ligand and its complexes were less toxic to RBCs as compared to doxorubicin. All the compounds showed moderate anticancer activities on MCF-7 (wild type) breast cancer cell lines.

Keywords: Oxopyrrolidine; DNA binding; Solution stability; Hemolysis assays; *In silico* studies; Anticancer profiles

*Corresponding author. Email: drimran_ali@yahoo.com

1. Introduction

Cancer incidence rates are increasing alarmingly due to many reasons [1, 2]. Despite several drugs available for treating cancer, the available anticancer drugs are often associated with serious side effects limiting their uses [3, 4]. Therefore, the need for no or less side effect exhibiting anticancer drugs, capable to control cancer even at late stages, still continues.

Nitrogen-containing heterocyclic compounds constitute one of the most important classes of pharmaceuticals in medicinal and agrochemical industries; about 60% of drugs are heterocyclic molecules [5]. Pyrrolidine and oxopyrrolidine moieties (figure 1) have served as basic structural motifs for the syntheses of many organic compounds with interesting biological properties. Exciting anticancer activities of heterocyclic compounds embedded with pyrrolidine and oxopyrrolidine units have been reported [6–8]. Ambaye *et al.* [9] reported that (R,S)3-{N,N-[bis-(2-chloroethyl)]-amino}-1-(2′-methoxyphenyl)-pyrrolidine-2,5-dione hydrochloride (***I***) (figure 2) showed antitumor activity against P388 (Menogaril-resistant mouse leukemia) and L1210 (mouse lymphocytic leukemia) cell lines; its co-administration with methotrexate resulted in significant increase of activity against these cancers.

Copper complexes have been investigated as potential anticancer agents during the last few decades. Copper is an essential cofactor in a number of enzymes and, therefore, may be less toxic than non-essential metals (platinum) [10]. A large number of copper(II) complexes have been synthesized and screened for their DNA binding efficiencies and anticancer activities [11–16]. Zhang and co-workers reported a copper–pyrrolidine dithiocarbamate complex [$Cu(PDTC)_2$], which was 10-fold more potent than cisplatin in suppressing the proliferation of BE(2)-C (human neuroblastoma) cell line. This complex arrested S-phase of cell cycle progression, induced cellular apoptosis and necrosis, and enhanced the expression of p53 protein [17]. Nickel forms an essential component of several enzymes, *viz.* urease,

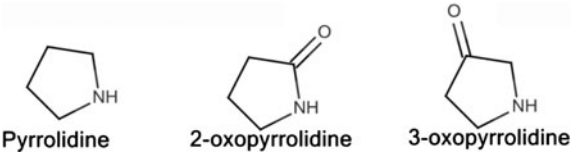

Figure 1. Chemical structure of pyrrolidine and 2- and 3-oxopyrrolidines.

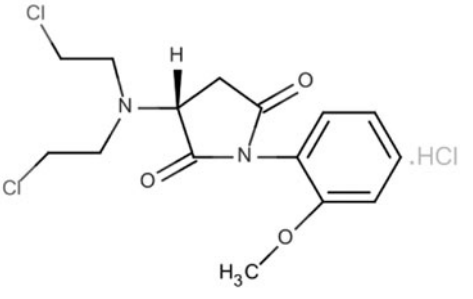

Figure 2. Chemical structure of (R,S)3-{N,N-[bis-(2-chloroethyl)]-amino}-1-(2′-methoxyphenyl)-pyrrolidine-2,5-dione hydrochloride (***I***).

carbon monoxide dehydrogenase and hydrogenase [18]. Many articles have reported DNA binding and anticancer potentials of nickel complexes owing to good affinity of Ni(II) for DNA and some DNA binding proteins [19–23]. Ruthenium complexes have been known for their anticancer potential [24–26]. As a result, a number of active ruthenium complexes emerged as potential new drugs [27–29]. Ru(III) complexes of NAMI-A and KP1019 (FFC14a) (figure 3) have already entered into clinical trials [30]. In view of these facts, an oxopyrrolidine based ligand was synthesized and separately complexed with Cu(II), Ni(II), and Ru(III) ions. The binding potential of the ligand and its complexes with Ct-DNA (Calf Thymus DNA) was studied by UV–vis absorption spectrophotometry. *In silico* studies of the ligand were carried out using AutoDock 4.2 tools. Molecular modeling and solution stabilities of the complexes were carried out by standard protocols. Hemolysis assays were carried out on rabbit RBCs and the anticancer profiles were determined on MCF-7 (wild type) cell lines. The results of these findings are presented herein.

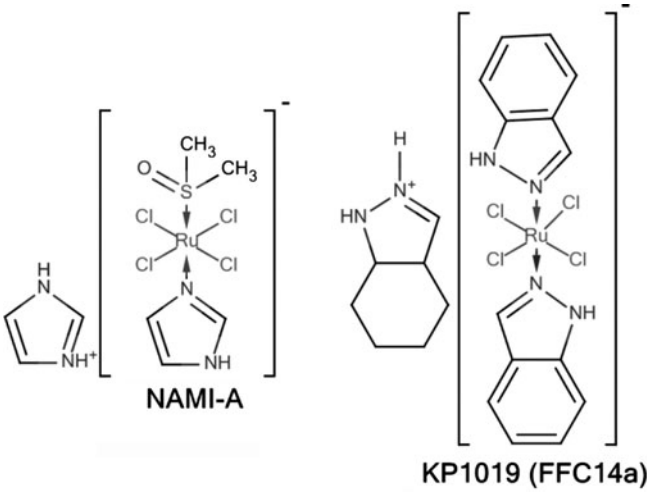

Figure 3. Chemical structures of Ru(III) complexes: NAMI-A and KP1019 (FFC14a).

2. Experimental setup

2.1. *Materials and methods*

All the reagents were of A.R. grades and used without purification. Solvents such as methanol, acetonitrile, chloroform, and hexane were of HPLC grade and procured from E. Merck, Mumbai, India. Pyroglutamic acid, *p*-chlorobenzaldehyde, and phosphorus oxychloride were purchased from Spectrochem, Mumbai, India. Acetic acid and sodium acetate were procured from Qualigens Fine Chemicals, Mumbai, India. $RuCl_3 \cdot 3H_2O$ was obtained from Avarice Lab. Pvt. Ltd, G.B. Nagar, India. $CuCl_2 \cdot 2H_2O$ and $NiCl_2 \cdot 6H_2O$ were purchased from E. Merck, Mumbai, India. Tris-(hydroxymethyl) aminomethane was supplied by Sisco Research Lab., Mumbai, India. Thiosemicarbazide, potassium hydroxide and disodium salt of Ct-DNA were purchased from S.D. Fine Chem. Ltd, New Delhi, India. Pre-coated aluminum silica gel 60 F_{254} thin layer plates were purchased from E. Merck, Germany.

Doxorubicin hydrochloride (an anticancer drug) was procured from Sigma-Aldrich, USA, and used as standard in hemolysis and anticancer assays. Human cancer cell lines *viz.* MCF-7 (wild type) were collected from the School of Pharmacy, College of Medicine, National Taiwan University. MTT [3-(4,5-dimethylthiazol-2-yl)-2,5-diphenyl tetrazolium bromide] was purchased from Sigma-Aldrich (St. Louis, MO, USA). Dulbecco's modified Eagle's medium (DMEM) and antibiotics/antimycotics were purchased from GIBCO (NY, USA). The fetal bovine serum (FBS) was obtained from HyClone (Ultah, USA).

The percentages of C, H, N, and S were determined by a Vario elemental analyzer (EL-III). UV–vis spectra were obtained on a Perkin Elmer Lambda 40 UV–vis spectrometer (CT 06859 USA). FT-IR spectra were recorded on a Perkin Elmer RXIFT system spectrometer (LR 64912C). ^{1}H NMR spectra were achieved with a Bruker 300 MHz instrument (DPX 300). ESI-mass spectra were recorded on micrOTOF-Q II spectrometer (10262). UV Cabinet was used to view TLC plates. Molar conductance measurements were carried out on a Decibel conductivity meter (DB-1038). A pH meter of Control Dynamics (APX 175 E/C) was used to record pH of solutions. Melting points were determined on a Veego instrument (REC-22038 A2). Millipore water was prepared by using a Millipore Milli-Q (Bedford, MA, USA) water purification system. *In silico* studies were performed by AutoDock 4.2 (Scripps Research Institute, USA) on Intel® core™ i3 CPU (3.2 GHz) with Windows XP operating system. Molecular modeling was performed with a semi-empirical PM3 as implemented in hyperchem 8.0 software program package (Hypercube, Inc., USA). Incubator for cell culture (MCO-15AC, Sanyo), centrifuge (CN2060, Hsiangtai Co.) and microplate photometer (Multiskan FC, Thermo Scientific) were used for carrying out the hemolysis and anticancer assays of the developed compounds.

2.2. *Synthesis of ligand (L)*

A stirred solution of pyroglutamic acid (5.94 g, 46.0 mM) in 40.0 mL glacial acetic acid was buffered with sodium acetate (7.55 g, 92.0 mM) and added to *p*-chlorobenzaldehyde (6.47g, 46.0 mM). The solution was refluxed with stirring for 6 h. The completion of the reaction was confirmed by TLC (methanol-chloroform, 70:30, v/v). The final reaction mixture was poured into ice-cold water, which resulted in the precipitation of the product (***I***). The precipitate was filtered through a Buchner funnel and thoroughly washed with cold water. Finally it was recrystallized from methanol and dried in a vacuum dessicator over fused calcium chloride. A mixture of (***I***) (0.503 g, 2.0 mM), thiosemicarbazide (0.183 g, 2.0 mM), and $POCl_3$ (1.0 mL) was gently refluxed for 30 min. The resulting mixture was cooled, 15.0 mL water was added, refluxed for an additional 4 h, and filtered. The filtrate obtained was neutralized with a saturated solution of potassium hydroxide and reduced to one-third of its volume on a rotary evaporator. The product was kept in a refregirator for precipitation of L. The ligand was washed with cold hexane and recovered from methanol. The schematic representation of the formation of (***I***) and L has been given in scheme 1.

(***I***): Yield: 63.0%, M wt. 251.5 Da, m.p. 212–214 °C, cream colored crystalline solid, anal. Calcd for $C_{12}H_{10}NO_3Cl$ (%): Calcd C (57.25), H (3.97), N (5.56); Found C (57.19) H (3.98) N (5.23); I.R. (KBr pellets, cm^{-1}): 2994.1 ν(O–H)carboxylic, 1735 ν(C=O)carboxylic, 1686.2 ν(C=O)amide, 1589.5 ν(N–H)bending, 1422.4 ν(C–N), 1315.5 ν(C–O)carboxylic, 761.1 ν(Ar–Cl); UV–vis (MeOH, nm): 222–232 ($n \rightarrow \sigma^*$), 257–273 ($\pi \rightarrow \pi^*$), 318–333 ($n \rightarrow \pi^*$); ^{1}H NMR (d_6-DMSO): 10.004 (s, COOH, 1H), 7.951 (d, Aromatic, 2H), 7.701 (d, Aromatic, 2H), 7.549 (s, =CH, 1H), 4.62 (dd, –CH, 1H), 3.389 (s, –NH, 1H), 2.34

(dd, >CH, 1H), 2.302 (dd, >CH, 1H); ESI-MS: *m/z* = 274.23 $[M + Na^+]^+$, 252.17 $[M + H]^+$, 229.32 $[M\text{-}COOH + Na^+]^+$, 133.12 $[M\text{-}C_7H_4Cl]^+$, 132.32 $[M\text{-}C_7H_5Cl]^+$.

L: Yield: 78.0%, M wt. 308.5 Da, m.p. 180–182 °C, banana yellow solid, anal. Calcd for $C_{13}H_{13}SN_4OCl$ (%): Calcd C (50.56), H (4.21), N (18.15), S (11.50); Found C (50.54), H (4.18), N (18.11), S (11.55); I.R. (KBr pellets, cm^{-1}): 3446 *ν*(–NH_2)asym., 1695 *ν*(C=O), 1647 *ν*(C=N), 1607 *ν*(N–H)bending, 1441 *ν*(C–N), 765.8 *ν*(Ar–Cl), 631 *ν*(C–S); UV–vis (MeOH, nm): 203–212 ($n \rightarrow \sigma^*$), 236–244 ($\pi \rightarrow \pi^*$), 312–337 ($n \rightarrow \pi^*$); ^{1}H NMR (d_6-DMSO): 8.224 (s, –NH, 1H), 8.043 (s, –NH_2, 2H), 7.964 (d, Aromatic, 2H), 7.859 (d, Aromatic, 2H), 7.299 (s, =CH, 1H), 4.387 (dd, –CH, 1H), 4.137 (dd, –CH, H), 3.976 (dd, –CH, H); ESI-MS: *m/z* = 633.48 $[2\,M + NH_4^+\text{-}2H]^+$, 409.96 $[M + 2\,K^+ + Na^+]^+$, 360.30 $[M + CH_3OH + NH_4^+ + 2H]^+$, 334.04 $[M + Na^+ + 3H]^+$, 230.02 $[M\text{-}C_2H_2SN_3 + Na^+\text{-}H]^+$, 214.5 $[M\text{-}C_2H_2SN_3 + 2H]^+$, 214.0 $[M\text{-}C_2H_2SN_3Cl + K^+ + 2H]^+$, 184.03 $[M\text{-}C_7H_5Cl]^+$, 183.03 $[M\text{-}C_7H_4Cl]^+$, 182.03 $[M\text{-}C_7H_3Cl]^+$.

2.3. *Synthesis of copper complex (CuL)*

A solution of copper chloride dihydrate (85.24 mg, 0.5 mM) in 15.0 mL methanol was added dropwise to a stirred solution of L (308.5 mg, 1.0 mM) in 20.0 mL methanol. The mixture was stirred at room temperature for 6 h. A precipitate of the metal complex formed and was collected by evaporation of solvent at room temperature. The solid complex (CuL) obtained was washed with hexane and then methanol. Finally, it was kept in a vacuum dessicator over fused calcium chloride.

Ni(II) and Ru(III) complexes were prepared by using $NiCl_2 \cdot 6H_2O$ and $RuCl_3 \cdot 3H_2O$, respectively, by a similar procedure. The complexes prepared were kept in a vacuum dessicator over fused calcium chloride. The schematic representation of the formation of CuL, NiL, and RuL is given in scheme 1.

CuL: Yield: 63.0%, M wt. 787.54 Da, m.p. decomposed over 110 °C, army green powder solid, Anal. Calcd for $[Cu(C_{13}H_{13}SN_4OCl)_2H_2O)_2]Cl_2$ (%): Calcd C (39.61), H (3.80), N (14.22), S (8.12); Found C (39.55), H (3.09), N (14.32), S (8.11); I.R. (KBr pellets, cm^{-1}): 3440.5 *ν*(–NH_2)asym., 1684.9 *ν*(C=O), 1618 *ν*(C=N), 1592.7 *ν*(N–H)bending, 1424.9 *ν*(C–N), 618 *ν*(C–S), 762.2 *ν*(Ar–Cl), 548.6 *ν*(Cu–O), 473.5 *ν*(Cu–N); UV–vis. (MeOH, nm): 225–243 ($n \rightarrow \sigma^*$), 252–272 (π–π^*), 312–329 ($n \rightarrow \pi^*$), 373–405 (charge transfer band), 806–815 ($^2T_{2g} \leftarrow {}^2E_g$); $\wedge_M$ (1×10^{-3} M, MeOH): 176.48 $\Omega^{-1}cm^2\,M^{-1}$ (1:2 electrolyte); ^{1}H NMR (d_6-DMSO): 7.889 (s, –NH, 2H), 7.515 (d, Aromatic, 4H), 7.215 (d, Aromatic, 4H), 7.045 (s, –NH_2, 4H), 6.875 (s, =CH, 2H), 4.310 (broad signal, 6H); ESI-MS: *m/z* = 811.55 $[M + Na^+ + H]^+$, 803.66 $[M + NH_4^+\text{-}2H]^+$, 783.52 $[M\text{-}4H]^+$, 766.90 $[M\text{-}Cl + NH_4^+\text{-}3H]^+$, 666.76 $[M\text{-}3Cl\text{-}H_2O + 2H]^+$, 664.76 $[M\text{-}3Cl\text{-}H_2O + H]^+$, 662.77 $[M\text{-}3Cl\text{-}H_2O\text{-}H]^+$, 594.26 $[M\text{-}2Cl\text{-}C_7H_5Cl + 2H]^+$, 593.26 $[M\text{-}2Cl\text{-}C_7H_5Cl + H]^+$, 592.26 $[M\text{-}2Cl\text{-}C_7H_5Cl]^+$, 488.90 $[M\text{-}3Cl\text{-}2H_2O\text{-}C_7H_5Cl\text{-}2NH_2]^+$, 487.91 $[M\text{-}3Cl\text{-}2H_2O\text{-}C_7H_5Cl\text{-}2NH_2\text{-}H]^+$, 486.91 $[M\text{-}3Cl\text{-}2H_2O\text{-}C_7H_5Cl\text{-}2NH_{2-2}H]^+$, 391.00 $[M\text{-}2Cl\text{-}H_2O\text{-}C_{13}H_{13}SN_4OCl + H]^+$, 389.00 $[M\text{-}2Cl\text{-}H_2O\text{-}C_{13}H_{13}SN_4OCl\text{-}H]^+$.

NiL: Yield: 57%, M wt. 782.69 Da, m.p. decomposed over 178 °C, arylide yellow powder solid, anal. Calcd for $[Ni(C_{13}H_{13}SN_4OCl)_2H_2O)_2]Cl_2$ (%): Calcd C (39.86), H (3.83), N (14.30), S (8.17); Found C (39.83), H (3.88), N (14.27), S (8.12); I.R. (KBr pellets, cm^{-1}): 3437.7 *ν*(–NH_2)asym., 1685 *ν*(C=O), 1642 *ν*(C=N), 1594.6 *ν*(N–H)bending, 1425 *ν*(C–N), 761.9 *ν*(Ar–Cl), 614 *ν*(C–S), 514.9 *ν*(Cu–O), 474.1 *ν*(Cu–N); UV–vis (MeOH, nm): 225–237 ($n \rightarrow \sigma^*$), 243–267 ($\pi \rightarrow \pi^*$), 303–319 ($n \rightarrow \pi^*$), 507–536 ($^3T_1g(F) \rightarrow {}^3A_2g(F)$,

890–899 ($^3T_2g(F) \rightarrow {}^3A_2g(F)$; $\wedge_M$ (1×10^{-3} M, MeOH): 181.39 $\Omega^{-1}cm^2\,M^{-1}$ (1 : 2 electrolyte); ^{1}H NMR (d_6-DMSO): 8.229 (s, –NH, 2H), 8.155 (d, Aromatic, 4H), 7.221 (d, Aromatic, 4H), 7.123 (s, $–NH_2$, 4H), 7.465 (s, =CH, 2H), 4.323 (broad peak, 6H); ESI-MS: *m/z* = 779.44 $[M\text{-}3H]^+$, 818.88 $[M + 2NH_4^+]^+$, 802.90 $[M + NH_4^+ + 2H]^+$, 748.24 $[M\text{-}2Cl + K^+\text{-}2H]^+$, 678.90 $[M\text{-}2Cl\text{-}2H_2O + 3H]^+$, 661.51 $[M\text{-}3Cl\text{-}2H_2O + Na^+\text{-}2H]^+$, 633.48 $[M\text{-}3Cl\text{-}2H_2O + Na]^+$, 334.04 $[M\text{-}Ni\text{-}2Cl\text{-}2H_2O\text{-}C_{13}H_{13}SN_4OCl + Na^+ + 2H]^+$, 275.94 $[M\text{-}Ni\text{-}3Cl\text{-}2H_2O\text{-}C_{13}H_{13}SN_4OCl + 2H]^+$, 274.94 $[M\text{-}Ni\text{-}3Cl\text{-}2H_2O\text{-}C_{13}H_{13}SN_4OCl + H]^+$, 273.94 $[M\text{-}Ni\text{-}3Cl\text{-}2H_2O\text{-}C_{13}H_{13}SN_4OCl]^+$, 271.94 $[M\text{-}Ni\text{-}3Cl\text{-}2H_2O\text{-}C_{13}H_{13}SN_4OCl\text{-}H]^+$, 124.07 $[M\text{-}Ni\text{-}2Cl\text{-}2H_2O\text{-}C_{13}H_{13}SN_4OCl\text{-}C_7H_5Cl\text{-}C_4H_4O + H]^+$.

RuL: Yield: 67.0%, M wt. 860.57 Da, m.p. decomposed over 222 °C, black powder solid, Anal. Calcd for $[Ru(C_{13}H_{13}SN_4OCl)_2H_2O)_2]Cl_3$ (%): Calcd C (36.25), H (3.48), N (13.01), S (7.43); Found C (36.17), H (3.39), N (13.03), S (7.45); I.R. (KBr pellets, cm^{-1}): 3429.9 *v*(-NH_2)asym., 1684.7 *v*(C=O), 1631 *v*(C=N), 1592.8 *v*(N–H), 1432 *v*(C–N), 764.1 *v*(Ar–Cl), 628 *v*(C–S), 522 *v*(Cu–O), 482.5 *v*(Cu–N); UV–vis (MeOH, nm): 212–225 ($n \rightarrow \sigma^*$), 239–261 ($\pi \rightarrow \pi^*$), 332–360 ($n \rightarrow \pi^*$), 517–589 ($^6A_{1g} \rightarrow {}^4T_{1g}$); $\wedge_M$ (1×10^{-3} M, MeOH): 310.12 $\Omega^{-1}cm^2\,M^{-1}$ (1:3 electrolyte); ^{1}H NMR (d_6-DMSO): 8.455 (s, –NH, 2H), 8.234 (d, Aromatic, 4H), 7.136 (d, Aromatic, 4H), 7.435 (s, $–NH_2$, 4H), 7.531 (s, =CH, 2H), 4.257 (broad peak, 6H); ESI-MS: *m/z* = 879.90 $[M + NH_4^+ + H]^+$, 858.21 $[M\text{-}2H]^+$, 793.24 $[M\text{-}3Cl + K^+]^+$, 740.23 $[M\text{-}3Cl\text{-}2H_2O + Na^+\text{-}H]^+$, 719.21 $[M\text{-}3Cl\text{-}2H_2O + H]^+$, 718.17 $[M\text{-}3Cl\text{-}2H_2O]^+$, 346.19 $[M\text{-}Ni\text{-}3Cl\text{-}2H_2O\text{-}C_{13}H_{13}SN_4OCl + 2H]^+$.

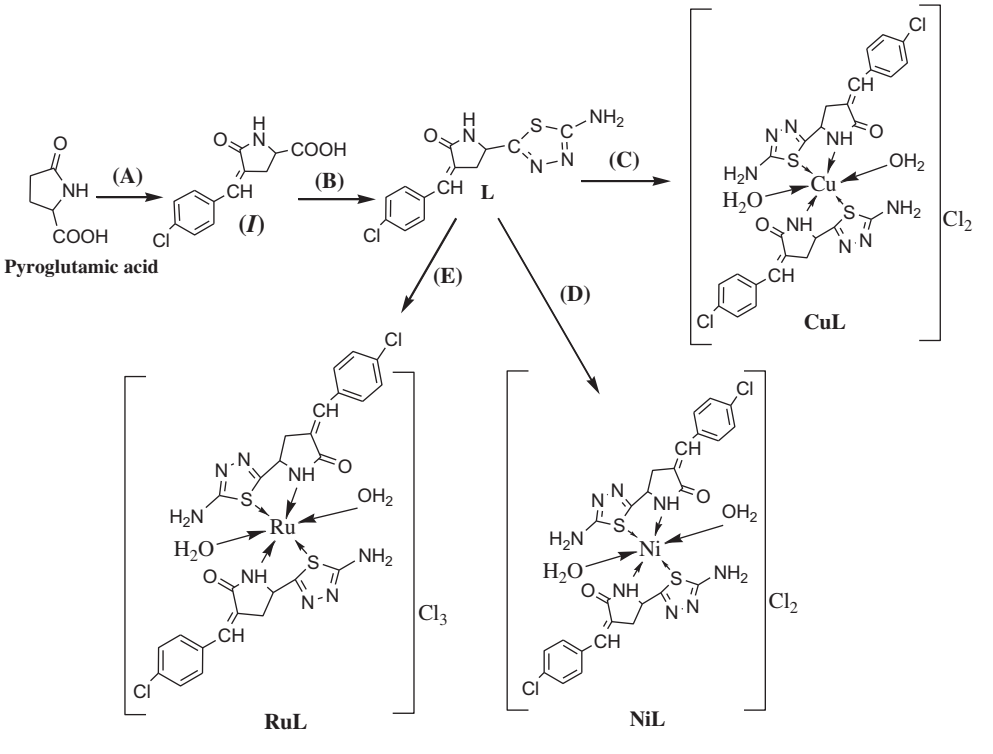

Scheme 1. Syntheses of L, CuL, NiL, and RuL. Reagents and conditions: (A) acetic acid, sodium acetate, *p*-chlorobenzaldehyde, reflux at 60 °C for 6 h, (B) thiosemicarbazide, $POCl_3$, water, reflux for 4 h, (C) $CuCl_2 \cdot 2H_2O$, stirring at room temp for 6 h, (D) $NiCl_2 \cdot 6H_2O$, stirring at room temp for 6 h, (E) $RuCl_3 \cdot 3H_2O$, stirring at room temp for 6 h.

2.4. *Solution stability*

A qualitative estimation of the stability of the complexes at physiological pH was obtained by monitoring their UV–vis spectra in 5% DMSO solutions of PBS at pH 7.4, over a period of 24 h. The solutions of the complexes (10^{-4} M) were prepared in 5% DMSO solutions of PBS at pH 7.4. The hydrolysis profiles of the complexes were assessed by recording their electronic spectra over 24 h at 25°C.

2.5. *Molecular modeling*

The molecular modeling studies were carried out with a semi-empirical PM3 as implemented in the Hyperchem 8.0 software [31, 32], a graphics program with features of structure building, geometry optimization, and quick molecular display. Polak−Ribiere was chosen as the minimization algorithm with RMS gradient of 0.1 kcal/(Å M) and 250 energy calculations were carried out.

2.6. *DNA binding*

UV–vis absorption spectrophotometry was used to assess the interactions of ligand and its complexes with Ct-DNA at 7.4 pH in double distilled water containing tris-(hydroxymethyl)-amino methane (Tris, 10^{-2} M). The concentration of the freshly prepared Ct-DNA solution was determined spectrophotometrically at 260 nm ($\varepsilon = 6600\ M^{-1}\ cm^{-1}$) [33]. The binding experiments were carried out by recording the absorbance changes on adding increasing concentrations of DNA (0.87×10^{-4}–1.47×10^{-4} M) against a fixed concentration of the ligand and its complexes (1.6×10^{-4} M); λ_{max} and absorbance values of pure DNA, ligand, and its complexes in buffer solutions were recorded. An amount of 2.0 mL of each solution of DNA and ligand or metal complex were mixed together and their λ_{max} and absorbance values were recorded. The absorption spectra were recorded after each addition of different concentrations of DNA solution (2.0 mL).

2.7. In silico *studies*

Docking studies of the ligand were performed by Intel® dual CPU (1.86 GHz) with Windows XP operating system. The 3-D structure of the ligand was drawn using Marwin sketch. The so-obtained 3-D structure was converted to the pdb file format. Ligand preparation was done by assigning Gastegier charges, merging non-polar hydrogens, and saving it in PDBQT file format using AutoDock Tools (ADT) 4.2 [34]. X-ray crystal structure of DNA (PDB ID: 1BNA) was obtained from the Protein Data Bank [35]. Using ADT 4.2, DNA was saved in PDB file format leaving heteroatoms (water). Gastegier charges were assigned to DNA and saved in PDBQT file format using ADT. Preparation of parameter files for grid and docking was done using ADT. Docking was performed with AutoDock 4.2 (Scripps Research Institute, USA), considering all the rotatable bonds of ligand as rotatable and receptor as rigid [36]. Grid box size of $60 \times 80 \times 110$ Å with 0.375 Å spacing was used that included the whole DNA. Docking to macromolecule was performed using an empirical-free energy function and Lamarckian Genetic Algorithm, with an initial population of 150 randomly placed individuals, a maximum number of 2,500,000 energy evaluations, a mutation rate of 0.02, and crossover rate of 0.80. Fifty independent docking runs were performed for each ligand and DNA−ligand adduct for lowest free energy of binding

conformation from the largest cluster and saved in PDBQT format. Docking results were analyzed using UCSF Chimera [37] for possible polar and hydrophobic interactions.

2.8. *Cytotoxicity profiles*

Pharmacological significance of the developed compounds was ascertained by evaluating their cytotoxicity profiles. Hemolysis effects and anticancer profiles of the compounds were evaluated on rabbit RBCs and MCF-7 cancer cell lines, respectively, using doxorubicin as reference drug. Both hemolysis and anticancer assays were carried out in triplicate as described below.

2.8.1. Hemolysis assays. The experimental procedure for evaluating the hemolysis behavior of the compounds is an adjustment of ASTM standard F-756-00 [38], which is based on colorimetric detection of Drabkin's solution. An amount of 1.5 mL of test compounds was incubated in 0.214 mL of dilute blood (0.1 mL rabbit whole blood mixed with 0.9 mL PBS) at 37 °C for 3 h. The hemoglobin in as-harvested plasma of rabbit blood was less than 220 μg mL^{-1} (basal level for hemolysis test) to confirm that fresh rabbit blood was used in the test. Following incubation, the solution was centrifuged at 3800 rpm for 15 min. To determine the supernatant hemoglobin, 0.8 mL of Drabkin's solution was added to 0.2 mL of supernatant and the sample was allowed to stand for 15 min. The amount of cyanmethemoglobin in the supernatant was measured by absorbance measurement at 540 nm and then compared to a standard curve (hemoglobin concentrations ranging from 32 to 1068 mg mL^{-1}). The percent hemolysis refers to the hemoglobin concentration in the supernatant of a blood sample not treated with test compounds to the obtained percentage of test compound-induced hemolysis. Additionally, the absorption of the test compounds was determined at 540 nm in order to eliminate the effect of absorption of test compounds. Finally, saline solution and double distilled water were used as negative and positive controls, respectively.

2.8.2. Anticancer assays. *In vitro* anticancer profiles were determined by testing L, CuL, NiL, and RuL against MCF-7 cell line by a cell viability assay (MTT assay) [39]. DMEM (low glucose), 10% FBS, and antibiotics/antimycotics formed the main constituents of the culture medium. MCF-7 cells were seeded in a 96-well plate at a density of 2×10^3 cells/well and were incubated at 37 °C under a humidified atmosphere containing 5% CO_2 for 24 h before assay. After that, the cells were further incubated in media containing various concentrations of the test compounds. After 24 h, the medium was removed and washed with PBS. About 20 μL of MTT solution was added to each well followed by 4 h of incubation at 37 °C. Subsequently, the medium was removed and 200 μL of DMSO were added. After shaking slowly twice for 5 s, the absorbance of each well was determined at 570 nm. The cell viability (%) was calculated as the ratio of the number of surviving cells in test compound-treated samples to that of control.

3. Results and discussion

The analytical and spectroscopic data of (***I***), L, CuL, NiL, and RuL supported their proposed structures. All the compounds were solids, stable to air, and soluble in

DMSO, DMF, and methanol. Pyroglutamic acid reacted with *p*-chlorobenzaldehyde in refluxing acetic acid buffered with sodium acetate to form (***I***). The carboxylic group of (***I***) cyclized with thiosemicarbazide in presence of $POCl_3$ to form oxopyrrolidine based ligand (L) (scheme 2). The compositions of the synthesized compounds were ascertained from their elemental analyses, molar conductance data, and ESI-MS spectra. The molar conductance values of CuL, NIL, and RuL were 176.48, 181.39, and 310.12 $\Omega^{-1}cm^2\,M^{-1}$. These values fall in electrolytic range with CuL and NiL existing as 1:2 electrolytes and RuL as 1:3 electrolyte. Therefore, the two chlorides in CuL and NiL existed outside their coordination spheres and thereby satisfying only the oxidation states of their respective metal ions. Similarly, the three chlorides existed outside the coordination sphere of RuL [40]. Finally, it can be assumed from the results of elemental analysis and ESI-MS spectra that 1:2 metal to ligand complexes were formed (scheme 1). The geometries of nickel and ruthenium complexes were octahedral while that for the copper complex was tetragonal. These geometries were well supported by their UV–vis spectra.

The formation of (***I***) was confirmed by the appearance of peaks due to (Ar–Cl), (C=O)amide, (C=O)carboxylic, (O–H)carboxylic, and (N–H)amide groups. The cyclization of the carboxylic group of (***I***) with thiosemicarbazide to form L was confirmed by the appearance of peaks due to (C=N) and (C–S) at 1647 and 631 cm^{-1}, respectively. Besides, the absence of peaks due to (C=O) and (O–H) portions of carboxylic group fully confirmed the cyclization and the formation of L. Coordination of copper(II), nickel(II), and ruthenium(III) to L was evident from the prominent frequency shifts to lower wavenumbers of (N–H) and (C–S) bands. Besides, the stretching frequencies for

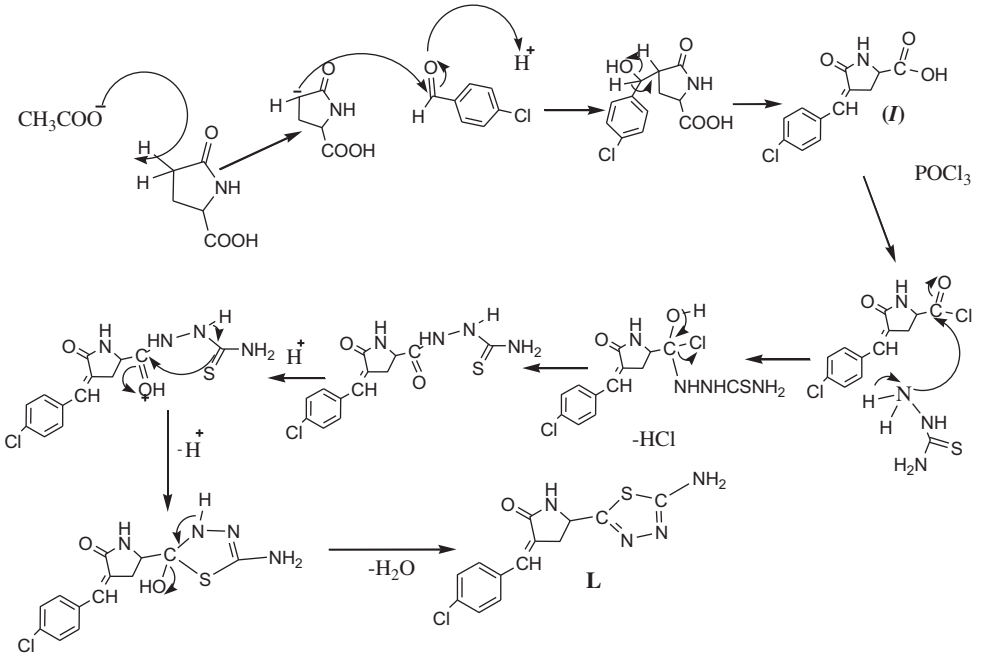

Scheme 2. Mechanistic presentation of the formation of L.

metal−ligand donor bonds (Cu–O, Cu–N, Ni–O, Ni–N, Ru–O and Ru–N) were observed in the spectra of all the complexes, suggesting coordination of metal ions with the ligand. Furthermore, the structures of (***I***), L, CuL, NiL, and RuL were well supported by their ^{1}H NMR spectra recorded in DMSO-d_6 as solvent and TMS as internal standard. The presence of a singlet at 10.004 ppm confirmed the presence of carboxylic group in (***I***). The aromatic protons in (***I***) were two sets of doublets at 7.701–7.951 ppm, whereas the signal due to the olefenic proton was observed as a singlet at 7.549 ppm. The absence of signal due to carboxylic proton in the ^{1}H NMR spectrum of L confirmed the cyclization of –COOH group of (***I***) with thiosemicarbazide. Aromatic protons in L were observed as two doublets at 7.859–7.964 ppm. The proton signals in the spectra of the complexes were very slightly shifted due to the coordinating effect of metal ions [41, 42]. The mass spectrum of L (figure 4) showed peaks at *m/z* values of 409.96, 360.30, and 334.04 corresponding to $[C_{13}H_{13}SN_4OCl + 2\,K^+ + Na^+]^+$, $[C_{13}H_{13}SN_4OCl + CH_3OH + NH_4^+ + 2H]^+$, and $[C_{13}H_{13}SN_4OCl + Na^+ + 3H]^+$, respectively. Besides, several fragmentation peaks were found at 230.02, 214.5, 214.0, 184.03, 183.03, and 182.03 corresponding to $[C_{13}H_{13}SN_4OCl\text{-}C_2H_2SN_3 + Na^+\text{-}H]^+$, $[C_{13}H_{13}SN_4OCl\text{-}C_2H_2SN_3 + 2H]^+$, $[C_{13}H_{13}SN_4OCl\text{-}C_2H_2SN_3Cl + K^+ + 2H]^+$, $[C_{13}H_{13}SN_4OCl\text{-}C_7H_5Cl]^+$, $[C_{13}H_{13}SN_4OCl\text{-}C_7H_4Cl]^+$, and $[C_{13}H_{13}SN_4OCl\text{-}C_7H_3Cl]^+$, respectively. The mass spectrum of CuL (figure 5) showed peaks at *m/z* values of 811.55, 803.66, 783.52, and 486.91 corresponding to $\{[Cu(C_{13}H_{13}SN_4OCl)_2H_2O)_2]Cl_2 + Na^+ + H\}^+$, $\{[Cu(C_{13}H_{13}SN_4OCl)_2H_2O)_2]Cl_2 + NH_4^+\text{-}2H\}^+$, $\{[Cu(C_{13}H_{13}SN_4OCl)_2H_2O)_2]Cl_{2-4}H\}^+$, and $\{[Cu(C_{13}H_{13}SN_4OCl)_2H_2O)_2]Cl_{2-3}Cl\text{-}2H_2O\text{-}C_7H_5Cl\text{-}2NH_{2-2}H]^+$, respectively. Several other fragmentation peaks were found in the spectrum of CuL further exploring its

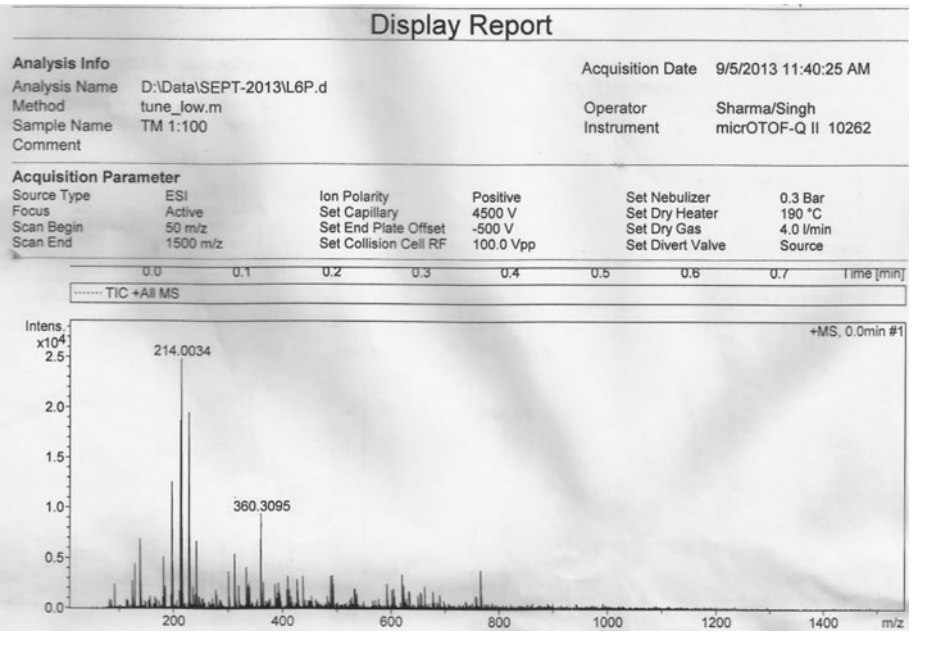

Figure 4. ESI-MS spectrum of L.

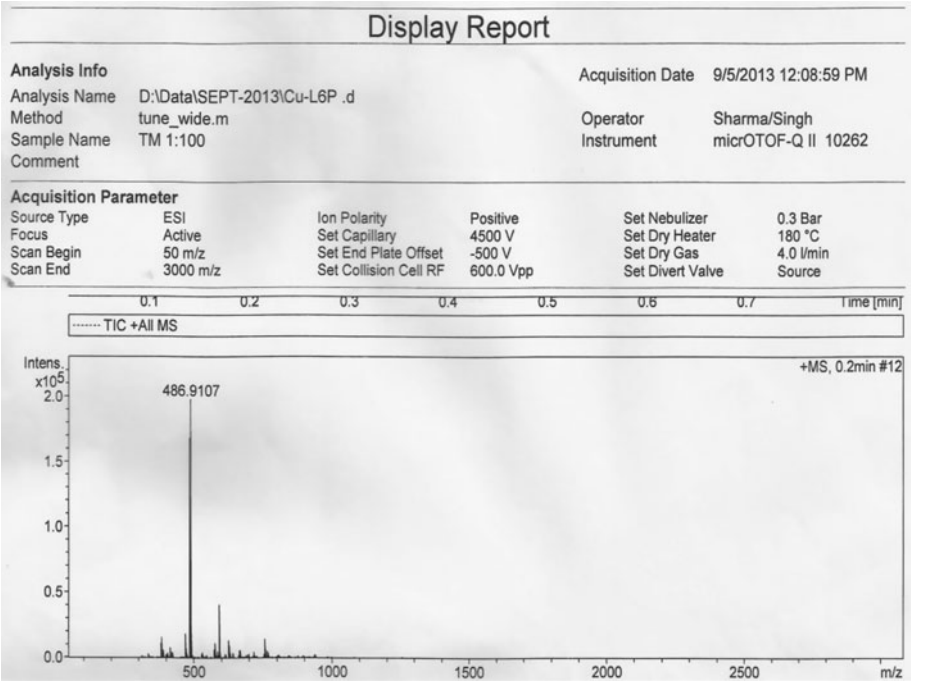

Figure 5. ESI-MS spectrum of CuL.

chemical structure. Mass spectra of NiL and RuL showed peaks at *m/z* values 779.44, 818.88 & 802.90, and 879.90 & 858.21 attributed to $\{[Ni(C_{13}H_{13}SN_4OCl)_2H_2O)_2]Cl_{2-3}H\}^+$, $\{[Ni(C_{13}H_{13}SN_4OCl)_2H_2O)_2]Cl_2 + 2NH_4^+\}^+$ & $\{[Ni(C_{13}H_{13}SN_4OCl)_2H_2O)_2]Cl_2 + NH_4^+ + 2H\}^+$, and $\{[Ru(C_{13}H_{13}SN_4OCl)_2H_2O)_2]Cl_3 + NH_4^+ + H\}^+$ & $\{[Ru(C_{13}H_{13}SN_4OCl)_2H_2O)_2]Cl_{3-2}H\}^+$, respectively. The UV–vis spectra of L (figure 6), CuL, NiL, and RuL (figure 7) were characterized by bands in the regions 203−243, 236−272, and 303−360 nm corresponding to the transitions $n \rightarrow \sigma^*$, $\pi \rightarrow \pi^*$, and $n \rightarrow \pi^*$, respectively. In addition to ligand-originated bands, additional absorption bands due to metal-originated d-d transitions and charge transfer spectra were observed in the spectra of the complexes, characteristic to their geometries. CuL showed absorption bands at 373–405 and 806–815 nm assigned to charge transfer bands and $^2T_{2g} \leftarrow ^2E_g$ transitions, respectively, indicating its tetragonally distorted octahedral geometry [43, 44]. NiL showed bands in the regions 507−536 and 890−899 nm assigned to $^3T_1g(F) \rightarrow ^3A_2g(F)$ and $^3T_2g(F) \rightarrow ^3A_2g(F)$ transitions, respectively, indicating its octahedral geometry [45–47]. Furthermore, RuL showed bands at 517−589 nm assigned to $^6A_{1g} \rightarrow ^4T_{1g}$ transition, respectively, indicating its octahedral geometry [48–50].

3.1. *Solution stability*

Aquation is an important process for the action of a large number of therapeutically active drugs, including the well-known KP1019 and NAMI-A [51–53]. UV–vis absorption spectroscopy is often used for the solution stability studies of complexes at physiological

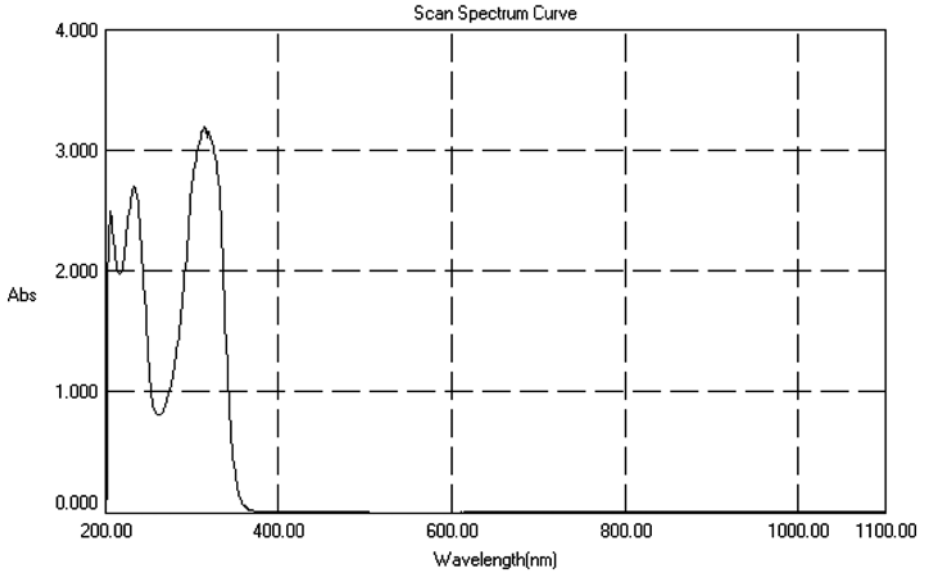

Figure 6. Electronic spectrum of L.

pH. CuL, NiL, and RuL displayed similar spectra in PBS (5% DMSO solutions) with no shifts in their intraligand bands (figure S1, see online supplementary material at http://dx.doi.org/10.1080/00958972.2014.931947.) after 24 h and also resisted precipitation over this time period. All these observations indicated the robust nature of the complexes [54–58].

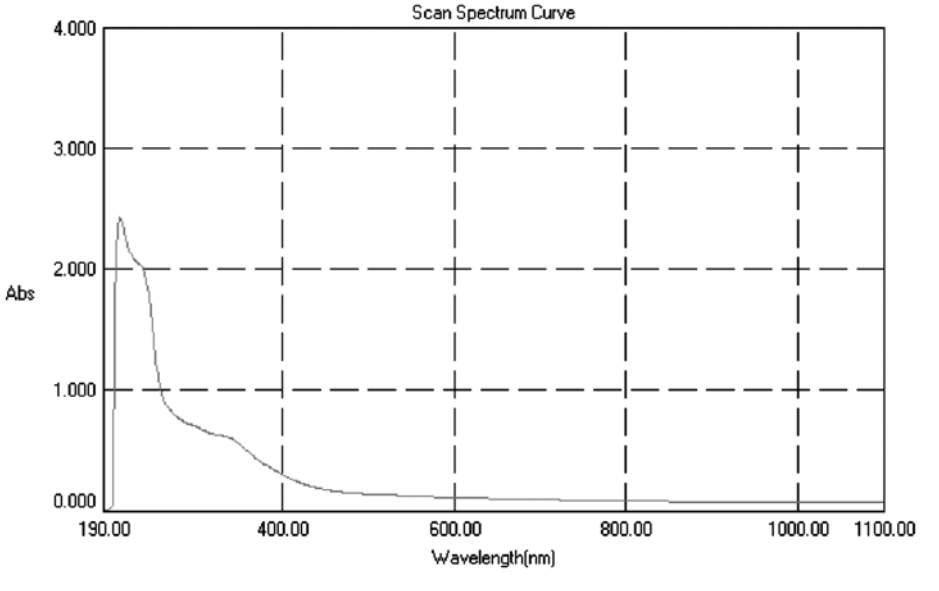

Figure 7. Electronic spectrum of RuL.

3.2. *Molecular modeling*

Molecular modeling exploits theoretical methods and computational techniques to model or mimic the behavior of molecules. Molecular modeling was used to have an insight into the structural information of complexes in the absence of crystal structure data. Energy-minimized configurations of complexes were achieved by the applications of molecular mechanics, which have become tools of increasing utility for the structural investigation of metal complexes [31, 59–61]. Molecular geometry is altered by energy minimization to lower the energy of the system. As a result of alteration of molecular geometry, the most stable configuration is achieved. The energy minimization process searches for a molecular structure wherein energy remains constant with infinitesimal changes in geometry. These studies were carried out by the use of semi-empirical PM3 as implemented in the Hyperchem 8.0 using Polak−Ribiere (conjugate gradient) algorithm keeping RMS gradient of 0.01 kcal/Å M. The ball and stick models of CuL, NiL and RuL are shown in figure 8. The total energies and heats of formation of CuL, NiL and RuL were –780,977.07, –767,316.31 and –725,585.09, and –1468.83, 952.86 and 3770.36 kJ M^{-1}, respectively (table 1). Besides, the surface areas and volumes of the modeled complexes ranged from 740.47 to 837.31 $Å^2$ and 1532.60 to 1638.71 $Å^3$, respectively (table 1).

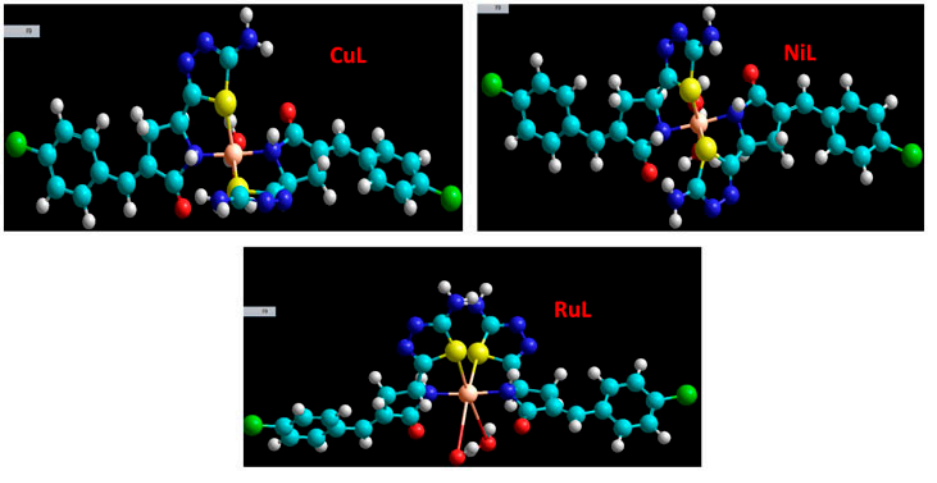

Figure 8. A perspective view of the ball and stick models of the energy-minimized structures of CuL, NiL, and RuL created through molecular modeling. Lone pairs are explicit for clarity. Nitrogen (blue), sulfur (yellow), carbon (cyan), oxygen (red), hydrogen (white), chlorine (green), copper, nickel, and ruthenium (orange). Chlorides outside coordination spheres have been ignored for the energy minimization process (see http://dx.doi.org/10.1080/00958972.2014.931947 for color version).

3.3. In silico *studies*

The present scenario witnesses high regards for combinatorial chemistry and virtual screening for their capacity of reducing the extremely time-consuming steps of organic and inorganic synthesis and biological screening of small molecule drugs. Molecular docking is an essential tool for the prediction of the interactions of drugs with various biological macromolecules at the supramolecular level [62]. B-DNA is the most common form of DNA with deep and wide major grooves and deep and narrow minor grooves. The specificity of the

base pairing between the two DNA strands gives distinct hydrogen bond acceptor/donor patterns in the major and minor grooves.

The docking studies of L were carried out using ADT 4.2. The results of molecular docking of L with DNA are shown in the form of a supramolecular model in figure 9(a) and (b). It can be visualized from the figure that the ligand preferred to enter into the DNA minor groove. The ligand interacted with DNA mainly through van der Waal's forces with $-31.21\ kJ\ M^{-1}$ as the van der Waal's energy. The docking energy of the ligand−DNA adduct was $-30.45\ kJ\ M^{-1}$, suggesting a good affinity of the reported ligand with DNA.

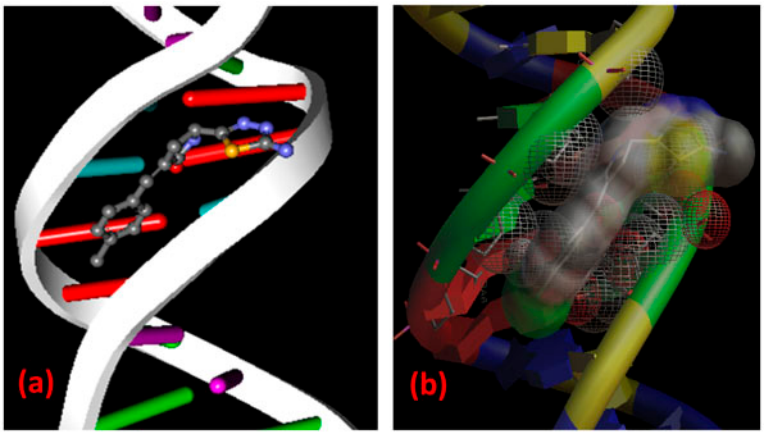

Figure 9. Docking images showing: (a) binding of L with DNA through minor groove, (b) van der Waal's interactions of L with the hydrophobic chains of DNA.

3.4. *DNA binding*

The affinities of molecules towards DNA are of great significance as DNA binding is a crucial step for action of a large number of anticancer drugs [63–65]. Ligands and transition metal complexes bind to DNA *via* both covalent and/or non-covalent interactions [66–69]. In case of covalent binding, one of the labile ligands of the complexes is replaced by a nitrogen base of DNA such as guanine N_7. Non-covalent interactions include intercalative, electrostatic, and groove (surface) binding either outside of the DNA helix or along major or minor grooves [70].

The changes in the spectral absorbance of DNA in the presence of ligands and complexes are evidence for interactions [71, 72]. The ratio of UV absorbance of the stock solution of Ct-DNA in buffer at 260 and 280 nm was greater than 1.80, revealing protein-free DNA [73]. The spectra depicting the interaction of DNA with L and CuL are shown in figures 10 and 11 and those of NiL and RuL in figures S2 and S3. Addition of increasing concentrations of DNA solutions, i.e. 0.87×10^{-4} M, 1.07×10^{-4}, 1.27×10^{-4} M, and 1.47×10^{-4} M, separately to the ligand and metal complex solutions (1.6×10^{-4} M) resulted in hyperchromic shifts of 4.54–22.50% (table 1). This suggested reversible binding to DNA, probably due to non-covalent interactions and the partial uncoiling and breakage of the helical structure of DNA exposing more bases [74]. The non-covalent interactions between the compounds and DNA might include hydrogen bonding, electrostatic attractions, and van der Waal's forces. Hydrogen bonding was supposed between the

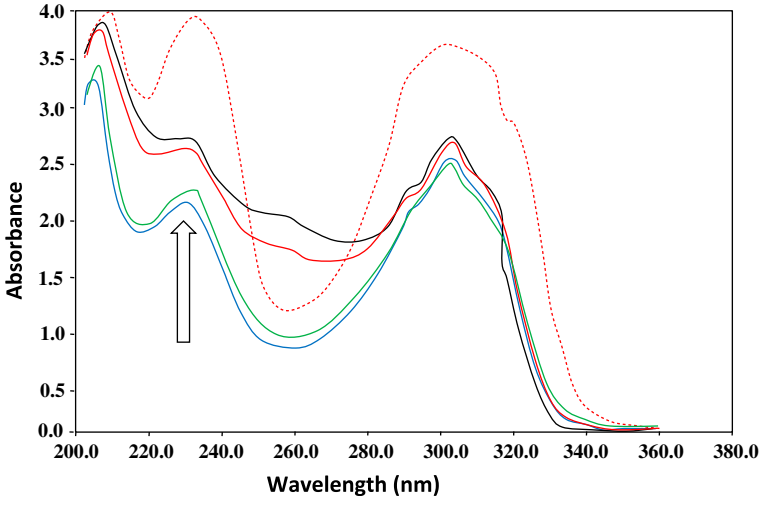

Figure 10. Absorption spectra of L (1.6×10^{-4} M) in the absence (red dashed line) and presence of increasing DNA concentrations; 0.87×10^{-4} M (blue), 1.07×10^{-4} M (green), 1.27×10^{-4} M (red) and 1.47×10^{-4} M (black) lines, respectively. Arrow indicates the hyperchromic shifts on increasing DNA concentrations ($0.87–1.47 \times 10^{-4}$ M) (see http://dx.doi.org/10.1080/00958972.2014.931947 for color version).

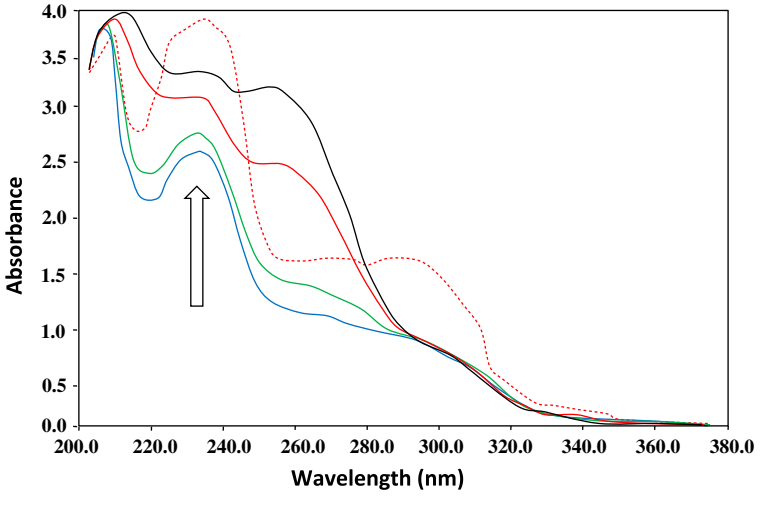

Figure 11. Absorption spectra of CuL (1.6×10^{-4} M) in the absence (red dashed line) and presence of increasing DNA concentrations; 0.87×10^{-4} M (blue), 1.07×10^{-4} M (green), 1.27×10^{-4} M (red) and 1.47×10^{-4} M (black) lines, respectively. Arrow indicates the hyperchromic shifts on increasing DNA concentrations ($0.87–1.47 \times 10^{-4}$ M) (see http://dx.doi.org/10.1080/00958972.2014.931947 for color version).

exposed base pairs of DNA in minor grooves with the free >C=O group and nitrogen of oxopyrrolidine ring and coordinated –NH– groups of the complexes. Electrostatic attractions might have occurred between the positive metal centers of complexes and the negatively charged DNA backbone. Moreover, van der Waal's interactions between methylene groups of the complexes and the hydrophobic moieties of DNA might also have enhanced binding. All these interactions lead to the formation of compound−DNA adducts.

Table 1. Percentage hyperchromism, binding constants, total energies, heats of formation, surface areas, and volumes of the compounds.

Compounds	% Hyperchromism	K_b (M^{-1})	Total energy (kJ M^{-1})	Heat of formation (kJ M^{-1})	Surface area (Å^2)	Volume (Å^3)
L	4.54	1.15×10^5				
CuL	5.76	1.67×10^5	−780,977.07	−1468.83	740.47	1555.14
NiL	4.61	1.87×10^5	−767,316.31	952.86	675.09	1532.60
RuL	22.50	1.007×10^6	−725,585.09	3770.36	837.31	1638.71

For a quantitative understanding of DNA binding affinities, the intrinsic binding constants (K_b) of L, CuL, NiL, and RuL were obtained by monitoring the changes in absorbance of $\pi \rightarrow \pi^*$ spectral band (236–272 nm) with increasing concentration of DNA, by using the equation [75],

$$[\mathrm{DNA}]/(\varepsilon_a - \varepsilon_f) = [\mathrm{DNA}]/(\varepsilon_b - \varepsilon_f) + 1/K_b(\varepsilon_b - \varepsilon_f)$$

where [DNA] is the concentration of DNA in base pairs, the apparent absorption coefficients ε_a, ε_f, and ε_b correspond to A_{obs}/[Compound], the extinction coefficient for the free compound, and the extinction coefficient for the compound in the fully bound form, respectively.

DNA binding constants (K_b) calculated for L, CuL, NiL, and RuL ranged from 1.15×10^5 to 1.007×10^6 M^{-1}, respectively, revealing a quite strong interaction of these compounds with DNA. Metal complexes often bind to DNA more efficiently as compared to their free ligands due to the additional charge on central metal ions and the presence of vacant d-orbitals [76]. Higher value of the DNA binding constant of RuL may be attributed the presence of tripositive ruthenium in this complex.

Table 2. A comparison of the DNA binding constants of copper, nickel, and ruthenium complexes reported with CuL (1.67×10^5 M^{-1}), NiL (1.87×10^5 M^{-1}), and RuL (1.007×10^6 M^{-1}) reported in this work.

S. No.	Cu(II) complexes (K_b)	Ni(II) complexes (K_b)	Ru(III) complexes (K_b)	References
1		4.57×10^5, 1.29×10^5, and 1.7×10^5		[77]
2			9.3×10^6, 7.8×10^6, and 8.2×10^6	[78]
3	1.03×10^5			[79]
4	6.87×10^3			[80]
5	2.0×10^5			[81]
6			8.5×10^5, 7.3×10^5, 4.3×10^5, and 7.5×10^4	[82]
7			2.9×10^4, 1.9×10^4, and 2.2×10^4	[83]
8	1.36×10^6, 4.32×10^5, 5.00×10^5 and 5.70×10^4			[84]
9	3.11×10^5 and 7.81×10^5			[85]
10			1.81×10^4 and 4.32×10^4	[86]
11		3.64×10^2, 4.13×10^2, 8.85×10^2, and 7.55×10^2		[87]
12		0.00027×10^5, 0.50030×10^5, 2.24×10^5, 3.18×10^5, 3.90×10^5, and 1.87×10^5		[88]
13			1.3×10^4 and 4.6×10^3	[89]
14			2.06×10^5 and 3.12×10^5	[90]

DNA binding constants of CuL, NiL, and RuL were compared with some copper(II), nickel(II), and ruthenium complexes reported in the literature (table 2). It was observed that CuL, NiL, and RuL displayed similar and higher binding constants than most of the similar metal-containing complexes. However, the binding constants of CuL, NiL, and RuL were lower than the classical intercalator ethidium bromide ($K_b = 7 \times 10^7\ M^{-1}$) [91]. Besides, the binding constants of CuL and NiL were lower than that of proflavin ($K_b = 4.1 \times 10^5\ M^{-1}$) [92], but RuL has a higher DNA binding constant as compared to proflavin.

3.5. *Hemolysis assays*

After the drugs enter into the animal body, they interact with the blood components, particularly RBCs (oxygen carrying blood cells). Hemolysis induced by drugs is usually rare but a serious toxicity, which may be due to direct toxicity of the drug, its metabolite, or an excipient in the formulation. Moreover, high drug concentrations can cause hemolysis even in normal adults. In individuals who are genetically predisposed to hemolysis, even smaller concentrations of drugs may cause hemolysis. Thrombocytopenia, neutropenia, hemolytic anemia, aplastic anemia, and macrocytic anemia are known to occur in some patients treated with drugs [93]. Therefore, US FDA has recommended hemolysis screening of drugs as a very important requirement of drug development [94].

In vitro hemolysis results of L, CuL, NiL, and RuL were carried out at 100.0 μg mL^{-1} concentration and are shown in figure 12. It is clear from this figure that L, CuL, NiL, and RuL exhibited 7, 17, 6, and 31% hemolysis, respectively. On the other hand, doxorubicin exhibited 42% hemolysis. Therefore, all the compounds were less toxic to RBCs as compared to doxorubicin.

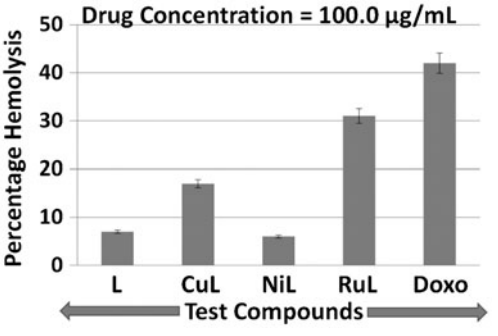

Figure 12. Percentage hemolysis of RBCs due to L, CuL, NiL, and RuL at 100.0 μg mL^{-1} concentration. Doxorubicin has been used as a reference drug.

3.6. *Anticancer profiles*

In vitro anticancer effects of L, CuL, NiL, and RuL were assessed from their percentage viabilities. The effects of the synthesized compounds on MCF-7 cells were determined at 0.0001–1.0 μg mL^{-1} concentration range with 10 × dilution factor. The percentage viabilities of the reported compounds are given in figure 13. It is clear from this figure that all the compounds were viable in the range of 93–103% at 0.0001 μg mL^{-1}. At higher concentration (0.001 μg mL^{-1}), viability was 95% for NiL and 98% for CuL, whereas L (94%) and

RuL (92%) showed better activities than doxorubicin (95% viability). Similarly, NiL (87% viability) showed activity equivalent to that of doxorubicin (87% viability) at 0.01 μg mL^{-1} concentration. Among the compounds screened at 0.1 μg mL^{-1}, L showed maximum pharmacological effect (84% viability), whereas the viabilities of CuL, NiL, and RuL were 95, 85, and 88%, respectively. Overall, the best pharmacological effects were observed with NiL at 1.0 μg mL^{-1} concentration (77% viability).

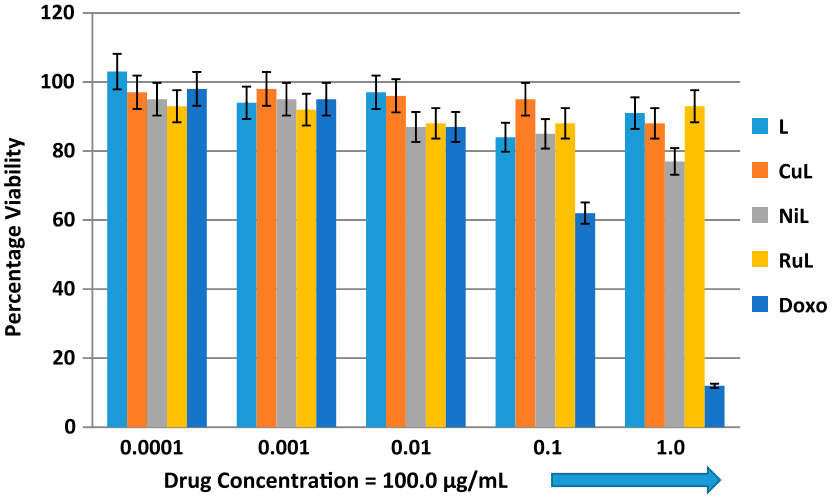

Figure 13. Percentage viabilities of L, CuL, NiL, and RuL with respect to the standard drug doxorubicin at 0.0001–1.0 μg mL^{-1} concentration.

3.7. *Future perspectives*

Despite the amazing scientific developments in almost every sphere of life, the cure for cancer still remains a challenge. The anticancer medications available in the market are unable to cure cancer, especially in its late stages. Drugs with rapid action, tissue specificity, good bioavailability, and minimum side effects are needed. Oxopyrrolidine-based metallodrugs with target selective action on cancer cells and tissues with minimum or no side effects can be obtained by trapping them into nano identities. Combination therapies are known to eliminate the chances of drug resistance of the cancer cells, since a cell cannot acquire resistance to two types of drugs simultaneously [95]. Therefore, it would be quite interesting for oxopyrrolidine-based metallodrugs to be investigated in combination therapies along with known anticancer drugs to develop novel drug combinations. The study of the molecular features of cancers may be quite helpful for the development of possible counter-attacking drugs [96]. Therefore, it would be quite helpful to study the relation of oxopyrrolidine-based metallodrugs with the molecular features of tumors, which may lead to the development of new and potent anticancer drugs in the future. Finally, designed multiple ligands (DMLs) (as multiple biological targets) may be helpful in the eradication of cancer [97]. Therefore, the development of oxopyrrolidine-based DMLs might be effective in the fight against cancer. Metallodrugs are a spark ignited in the rational design and development of anticancer drugs.

4. Conclusion

The facile syntheses of an oxopyrrolidine-based ligand and its copper(II), nickel(II), and ruthenium(III) complexes have been described. The complexes were stable to air and have good stabilities in 5% DMSO solutions of PBS at physiological pH. The values of DNA binding constants indicate strong binding ability of the compounds. The complexes exhibited higher binding ability as compared to the free ligand; binding constants of the complexes are higher than and comparable to complexes of same metals reported in the literature. DNA−complex adducts were proposed to be stabilized mainly by hydrogen bonding, van der Waal's, and electrostatic attractions. Hemolysis assays confirmed that the ligand and its complexes were less toxic to RBCs than doxorubicin. Overall, NiL stood as the best anticancer candidate with the least hemolysis effect and the minimum viability among the compounds screened. Anticancer activities of the reported complexes were not consistent with their DNA binding abilities, which ruled out DNA binding as the mechanism of action of these compounds. Briefly, the results presented in this article encourage further examination of the reported compounds towards other cell lines.

Acknowledgements

The authors extend their appreciation to the Deanship of Scientific Research at King Saud University for funding this work. One of the authors (Waseem Ahmad Wani) is thankful to the University Grants Commission (UGC), New Delhi, for providing UGC-BSR research fellowship.

References

[1] I. Ali, W.A. Wani, K. Saleem. *Cancer Ther.*, **8**, 56 (2011).
[2] I. Ali Rahis-Uddin, K. Saleem, H.Y. Aboul-Enein, A. Rather. *Cancer Ther.*, **8**, 6 (2011).
[3] I. Ali Rahis-Uddin, K. Saleem, M.A. Rather, W.A. Wani, A. Haque. *Curr. Cancer Drug Targets*, **11**, 135 (2011).
[4] N. Shah, D.S. Dizon. *Future Oncol.*, **5**, 33 (2009).
[5] V. Sridharan, P.A. Suryavanshi, J.C. Menéndez. *Chem. Rev.*, **111**, 7157 (2011).
[6] C. Bello, M. Cea, G. Dal Bello, A. Garuti, I. Rocco, G. Cirmena, E. Moran, A. Nahimana, M.A. Duchosal, F. Fruscione, P. Pronzato, F. Grossi, F. Patrone, A. Ballestrero, M. Dupuis, B. Sordat, A. Nencioni, P. Vogel. *Bioorg. Med. Chem.*, **18**, 3320 (2010).
[7] H. Fiaux, D.A. Kuntz, D. Hoffman, R.C. Janzer, S. Gerber-Lemaire, D.R. Rose, L. Juillerat-Jeanneret. *Bioorg. Med. Chem.*, **16**, 7337 (2008).
[8] I. Ali, W.A. Wani, K. Saleem, M.F. Hsieh. *Chem. Pap.*, **68**, 540 (2014).
[9] R.Y. Ambaye, M.A. Indap, S.D. Naik. *J. Cancer Res. Clin. Oncol.*, **115**, 379 (1989).
[10] C. Marzano, M. Pellei, F. Tisato, C. Santini. *Anticancer Agents Med. Chem.*, **9**, 185 (2009).
[11] I. Ali, W.A. Wani, K. Saleem, M.F. Hseih. *Polyhedron*, **56**, 134 (2013).
[12] R. Loganathan, S. Ramakrishnan, E. Suresh, A. Riyasdeen, M.A. Akbarsha, M. Palaniandavar. *Inorg. Chem.*, **51**, 5512 (2012).
[13] K. Saleem, W.A. Wani, A. Haque, M.N. Lone, M.F. Hsieh, M.A. Jairajpuri, I. Ali. *Future Med. Chem.*, **5**, 135 (2013).
[14] Y. Xiao, C. Bi, Y. Fan, S. Liu, X. Zhang, D. Zhang, Y. Wang, R. Zhu. *J. Coord. Chem.*, **62**, 3029 (2009).
[15] Y.J. Zheng, X.W. Li, Y.T. Li, Z.Y. Wu, C.W. Yan. *J. Coord. Chem.*, **65**, 3530 (2012).
[16] V. Mathew, J. Keshavayya, V.P. Vaidya, M.H.M. Khan. *J. Coord. Chem.*, **61**, 2629 (2008).
[17] H. Zhang, J.S. Wu, F. Peng. *Anti-Cancer Drug*, **19**, 125 (2008).
[18] T. Rau, R. van Eldik. In *Metal Ions in Biological Systems*, H. Sigel, A. Sigel (Eds), pp. 339–378, Marcel Dekker, New York (1996).
[19] F. Zhang, Q.Y. Lin, X.L. Zheng, L.L. Zhang, Q. Yang, J.Y. Gu. *J. Fluoresc.*, **22**, 1395 (2012).
[20] H.A. El-Boraey. *Spectrochim. Acta A Mol. Biomol. Spectrosc.*, **97**, 255 (2012).

[21] S. Shobana, J. Dharmaraja, S. Selvaraj. *Spectrochim. Acta A Mol. Biomol. Spectrosc.*, **107**, 117 (2013).
[22] R. Prabhakaran, P. Kalaivani, R. Huang, P. Poornima, V. Vijaya Padma, F. Dallemer, K. Natarajan. *J. Biol. Inorg. Chem.*, **18**, 233 (2013).
[23] C.W. Hsu, C.F. Kuo, S.M. Chuang, M.H. Hou. *Biometals*, **26**, 1 (2013).
[24] R. Rudolph. *Arch. Exp. Veterinaermed.*, **25**, 925 (1971).
[25] L.J. Anghileri. *Z. Krebsforsch. Klin. Onkol. Cancer Res. Clin. Oncol.*, **83**, 213 (1975).
[26] M.J. Clarke. *Met. Ions Biol. Syst.*, **11**, 231 (1980).
[27] L. He, S.Y. Liao, C.P. Tan, R.R. Ye, Y.W. Xu, M. Zhao, L.N. Ji, Z.W. Mao. *Chem. Eur. J.*, **19**, 12152 (2013).
[28] R.K. Koiri, A. Mehrotra, S.K. Trigun. *Med. Hypoth.*, **80**, 841 (2013).
[29] A. Levina, J.B. Aitken, Y.Y. Gwee, Z.J. Lim, M. Liu, A.M. Singharay, P.F. Wong, P.A. Lay. *Chem. Eur. J.*, **19**, 3609 (2013).
[30] D. Pluim, R.C. van Waardenburg, J.H. Beijnen, J.H. Schellens. *Cancer Chemother. Pharmacol.*, **54**, 71 (2004).
[31] P.R. Reddy, N. Raju. *Polyhedron*, **44**, 1 (2012).
[32] HyperChem Version 8.0 Hypercube, Inc. USA.
[33] M.F. Reichmann, S.A. Rice, C.A. Thomas, P. Doty. *J. Am. Chem. Soc.*, **76**, 3047 (1954).
[34] M.F. Sanner. *J. Mol. Graph Model.*, **17**, 57 (1999).
[35] Protein Data Bank. Available online at: http://www.rcsb.org/pdb.
[36] G.M. Morris, G.S. Goodsell, R.S. Halliday, R. Huey, W.E. Hart, R.K. Belew, A.J. Olson. *J. Comput. Chem.*, **19**, 1639 (1998).
[37] E.F. Pettersen, T.D. Goddard, C.C. Huang, G.S. Couch, D.M. Greenblatt, E.C. Meng, T.E. Ferrin. *J. Comput. Chem.*, **25**, 1605 (2004).
[38] ASTM F756-00, *Standard Practice for Assessment of Hemolytic Properties of Materials*, ASTM International, West Conshohocken, PA (2000). doi: 10.1520/F0756-00.
[39] T. Mosman. *J. Immunol. Methods*, **65**, 55 (1983).
[40] I. Ali, W.A. Wani, K. Saleem. *Synth. React. Inorg. Met-Org. Nano-Met. Chem.*, **43**, 1 (2013).
[41] A. Chaudhary, R.V. Singh. *Ind. J. Chem.*, **43**, 2529 (2004).
[42] W. Kemp. *Organic Spectroscopy*, Macmillan, London (1975).
[43] C.H. Krushna, C.M. Mahapatra, A.K. Dash. *J. Inorg. Nucl. Chem.*, **39**, 1253 (1977).
[44] N.N. Greenwood, A. Earnshaw. *Chemistry of the Elements*, Pergamon Press, New York (1984).
[45] R. Atkins, G. Brewer, E. Kokot, G.M. Mocler, E. Sinn. *Inorg. Chem.*, **24**, 127 (1985).
[46] B.N. Figgis, J. Lewis. *Modern Coordination Chemistry*, Interscience, New York (1960).
[47] O.M. Adly. *Spectrochim. Acta A Mol. Biomol. Spectrosc.*, **95**, 483 (2012).
[48] A.B.P. Lever. *Inorganic Electronic Spectroscopy*, 2nd Edn, Elsevier, Amsterdam (1984).
[49] M.M.T. Khan, D. Srinivas, R.I. Khureshy, N.H. Khan. *Inorg. Chem.*, **29**, 2320 (1990).
[50] S.N. Pal, S. Pal. *Eur. J. Inorg. Chem.*, **2003**, 4244 (2003).
[51] A. Kung, T. Pieper, R. Wissiack, E. Rosenberg, B.K. Keppler. *J. Biol. Inorg. Chem.*, **6**, 292 (2001).
[52] M. Groessl, C.G. Hartinger, P.J. Dyson, B.K. Keppler. *J. Inorg. Biochem.*, **102**, 1060 (2008).
[53] M. Bacac, A.C. Hotze, K. van der Schilden, J.G. Haasnoot, S. Pacor, E. Alessio, G. Sava, J. Reedijk. *J. Inorg. Biochem.*, **98**, 402 (2004).
[54] F. Arjmand, A. Jamsheera, D.K. Mohapatra. *J. Photochem. Photobiol. B: Biol.*, **121**, 75 (2013).
[55] C. Tan, S. Hu, J. Liu, L. Ji. *Eur. J. Med. Chem.*, **46**, 1555 (2011).
[56] F. Arjmand, M. Aziz, M. Chauhan. *J. Inclusion Phenom. Macrocycl. Chem.*, **61**, 265 (2008).
[57] L. Giovagnini, S. Sitran, M. Montopoli, L. Caparrotta, M. Corsini, C. Rosani, P. Zanello, Q.P. Dou, D. Fregona. *Inorg. Chem.*, **47**, 6336 (2008).
[58] G.E. Buchel, I.N. Stepanenko, M. Hejl, M.A. Jakupec, B.K. Keppler, V.B. Arion. *Inorg. Chem.*, **50**, 7690 (2011).
[59] B.K. Singh, H.K. Rajour, A. Prakash. *Spectrochim. Acta A Mol. Biomol Spectrosc.*, **94**, 143 (2012).
[60] Y.C. Chan, A.S.M. Ali, M. Khairuddean, K.Y. Khaw, V. Murugaiyah, A. Basiri. *Chin. Chem. Lett.*, **24**, 609 (2013).
[61] D.M. Abd El-Aziz, S.E.H. Etaiw, E.A. Ali. *J. Mol. Struct.*, **1048**, 487 (2013).
[62] I. Ali, A. Haque, K. Saleem, M.F. Hsieh. *Bioorg. Med. Chem.*, **21**, 3808 (2013).
[63] H.K. Liu, P.J. Sadler. *Acc. Chem. Res.*, **44**, 349 (2011).
[64] K.E. Erkkila, D.T. Odom, J.K. Barton. *Chem. Rev.*, **99**, 2777 (1999).
[65] H.T. Chifotides, K.R. Dunbar. *Acc. Chem. Res.*, **38**, 46 (2005).
[66] G. Psomas. *J. Inorg. Biochem.*, **102**, 1798 (2008).
[67] M. Carter, A.J. Bard, M. Rodriguez. *J. Am. Chem. Soc.*, **111**, 8901 (1989).
[68] J. Wang. *Anal. Chim. Acta*, **469**, 63 (2002).
[69] J.M. Kelly, A.B. Tossi, D.J. McConnell, C. OhUigin. *Nucleic Acids Res.*, **13**, 6017 (1985).
[70] A.M. Pyle, J.P. Rehmann, R. Meshoyrer, C.V. Kumar, N.J. Turro, J.K. Barton. *J. Am. Chem. Soc.*, **111**, 3051 (1989).
[71] Z.D. Xu, H. Liu, S.L. Xiao, M. Yang, X.H. Bu. *J. Inorg. Biochem.*, **90**, 79 (2002).
[72] Y. Wang, Z.Y. Yan. *Transition Met. Chem.*, **30**, 902 (2005).

[73] J. Marmur. *J. Mol. Biol.*, **3**, 208 (1961).
[74] C.J. Bernadou, B. Meunier. *Adv. Inorg. Chem.*, **45**, 251 (1998).
[75] A. Wolfe, G.H.J. Shimer, T. Meehan. *Biochemistry*, **26**, 6392 (1987).
[76] M. Chauhan, F. Arjmand. *Chem. Biodivers.*, **3**, 660 (2006).
[77] D.D. Li, Z.W. Tao. *J. Coord. Chem.*, **66**, 4237 (2013).
[78] P. Zhao, J. Li, L.J. Yang, J.Z. Lu, H.M. Guo, L.N. Ma, B.H. Ou. *J. Coord. Chem.*, **66**, 4220 (2013).
[79] T.T. Xing, S.H. Zhan, Y.T. Li, Z.Y. Wu, C.W. Yan. *J. Coord. Chem.*, **66**, 3149 (2013).
[80] C.Z. Xie, M.M. Sun, S.H. Li, X.T. Zhang, X. Qiao, Y. Ouyang, J.Y. Xu. *J. Coord. Chem.*, **66**, 3891 (2013).
[81] X.L. Wang, M. Jiang, Y.T. Li, Z.Y. Wu, C.W. Yan. *J. Coord. Chem.*, **66**, 1985 (2013).
[82] M. Shilpa, S. Devi, P. Nagababu, N.L. Latha, R. Pallela, V.R. Janapala, K. Aravind, S. Satyanarayana. *J. Coord. Chem.*, **66**, 1661 (2013).
[83] S. Sathiyaraj, R.J. Butcher, C. Jayabalakrishnan. *J. Coord. Chem.*, **66**, 580 (2013).
[84] Z.L. Hua, W.W. Na, W. Yuan, S. Guang. *J. Coord. Chem.*, **66**, 227 (2013).
[85] S. Anbu, A. Killivalavan, E.C.B.A. Alegria, G. Mathan, M. Kandaswamy. *J. Coord. Chem.*, **66**, 3989 (2013).
[86] N. Ljubijankic, A. Zahirovic, E. Turkusic, E. Kahrovic. *Croat. Chem. Acta*, **86**, 215 (2013).
[87] V.C. da Silveira, H. Benezra, J.S. Luz, R.C. Georg, C.C. Oliveira, A.M. Ferreira. *J. Inorg. Biochem.*, **105**, 1692 (2011).
[88] P. Jaividhya, R. Dhivya, M.A. Akbarsha, M. Palaniandavar. *J. Inorg. Biochem.*, **114**, 94 (2012).
[89] T.S. Kamatchi, N. Chitrapriya, H. Lee, C.F. Fronczek, F.R. Fronczek, K. Natarajan. *Dalton Trans.*, 2066 (2012).
[90] Y.J. Liu, C.H. Zeng, H.L. Huang, L.X. He, FH Wu. *Eur. J. Med. Chem.*, **45**, 564 (2010).
[91] M.J. Waring. *J. Mol. Biol.*, **13**, 269 (1965).
[92] Y. Baba, C.L. Beathy, A. Kagemato, C. Gebelien. *Biological Activity of Polymers,* ACS Symposium Series, Vol. 186, American Chemical Society, Washington, DC (1962).
[93] M.M. Lubran. *Ann. Clin. Lab. Sci.*, **19**, 114 (1989).
[94] FDA Guidance for Industry-Nonclinical Studies for the Safety Evaluation of Pharmaceutical Excipients, 2005. Available online at: http:/www.fda.gov/downloads/drugs/guidanceComplianceRegulatoryInformation/Guidances/ucm079250.pdf.
[95] I. Ali, W.A. Wani, A. Haque, K. Saleem. *Future Med. Chem.*, **5**, 961 (2013).
[96] A. Urruticoechea, R. Alemany, J. Balart, A. Villanueva, F. Vinals, G. Capella. *Curr. Pharm. Des.*, **16**, 3 (2010).
[97] N.M. O'Boyle, M.J. Meegan. *Curr. Med. Chem.*, **18**, 4722 (2011).